Title
Cabozantinib Resolves Bone Scans in Tumor-Naïve Mice Harboring Skeletal Injuries

Permalink
https://escholarship.org/uc/item/88x7r5jj

Journal
Molecular Imaging, 13(8)

ISSN
1535-3508

Authors

Doran, Michael G
Spratt, Daniel E
Wongvipat, John
et al.

Publication Date
2014-10-01

DOI
10.2310/7290.2014.00026

Peer reviewed

Cabozantinib Resolves Bone Scans in Tumor-Naïve Mice Harboring Skeletal Injuries

Michael G. Doran, **Daniel E. Spratt**, **John Wongvipat**, **David Ulmert**, **Brett S. Carver**, **Charles L. Sawyers**, and **Michael J. Evans**

Department of Radiology, Radiation Oncology Service, Human Oncology and Pathogenesis Program, Urology Service of the Department of Surgery, and the Howard Hughes Medical Institute, Memorial Sloan-Kettering Cancer Center, New York, NY; Department of Urology, Lund University, Skåne University Hospital, Lund, Sweden; and Department of Radiology and Biomedical Imaging, University of California, San Francisco, San Francisco, CA

Abstract

The receptor tyrosine kinase inhibitor cabozantinib (XL184, BMS-907351 Cometriq) has displayed impressive clinical activity against several indications, culminating in its recent approval for medullary thyroid cancer. Among malignancies with tropism for the bone (prostate, breast), one striking feature of early clinical reports about this drug has been the rapid and complete resolution of bone scans, a phenomenon almost never observed even among therapies already shown to confer survival benefit. In castration-resistant prostate cancer, not all conventional response indicators change as dramatically posttreatment, raising the possibility that cabozantinib may impair the ability of bone-seeking radionuclides to integrate within the remodeling bone. To test this hypothesis, we surgically induced bone remodeling via physical insult in non–tumor-bearing mice and performed ^{18}F–sodium fluoride (^{18}F-NaF) positron emission tomographic (PET) and technetium 99m–methylene diphosphonate (^{99m}Tc-MDP) single-photon emission computed tomographic (SPECT) scans pre- and posttreatment with cabozantinib and related inhibitors. A consistent reduction in the accumulation of either radiotracer at the site of bone remodeling was observed in animals treated with cabozantinib. Given that cabozantinib is known to inhibit several receptor tyrosine kinases, we drugged animals with various permutations of more selective inhibitors to attempt to refine the molecular basis of bone scan resolution. Neither the vascular endothelial growth factor receptor (VEGFR) inhibitor axitinib, the MET inhibitor crizotinib, nor the combination was capable of inhibiting ^{18}F-NaF accumulation at known bioactive doses. In summary, although the mechanism by which cabozantinib suppresses radionuclide incorporation into foci undergoing bone remodeling remains unknown, that this phenomenon occurs in tumor-naïve models indicates that caution should be exercised in interpreting the clinical significance of this event.

The Receptor Tyrosine Kinase (RTK) inhibitor cabozantinib was developed for clinical use by Exelixis, Inc. (South San Francisco, CA) and Bristol-Myers Squibb (New York, NY)

Address reprint requests to: Michael J. Evans, PhD, Department of Radiology and Biomedical Imaging, University of California, San Francisco, 185 Berry Street, Lobby 6 Suite 350, San Francisco, CA 94143-0946; michael.evans@ucsf.edu.

owing to encouraging antitumor effects in multiple preclinical cancer models, as well as its favorable oral bioavailability.[1,2] To date, at least 12 clinical trials are active or recruiting for eight indications, reflecting the ongoing enthusiasm for this drug since its regulatory approval in 2012 for medullary thyroid cancer.[3,4]

Because several of the RTKs targeted by cabozantinib are thought to contribute in part to the pathobiology of castration-resistant prostate cancer (CRPC),[5] a phase I/II clinical trial was initiated, and the findings were disclosed as abstracts or in peer-reviewed literature from 2011 to 2013.[6–9] Among the evidence of effective therapeutic intervention (delay in progression-free survival, pain palliation, regression in soft tissue lesions, decreases in serum markers of bone turnover) was the remarkable degree of partial or complete resolution of foci posttreatment detected with technetium 99m–methylene diphosphonate (^{99m}Tc-MDP) single-photon emission computed tomography (SPECT), colloquially referred to as the "bone scan" (approximately 68% of patients showed some resolution in their bone scans).[7]

Given that bone scans are routinely used at centers worldwide as the gold standard to monitor skeletal tumor burden and the rate of disease progression through bone, there is justifiable enthusiasm for achieving such a milestone. Nevertheless, the rapid kinetics of the effect—bone scan resolution occurs within weeks posttreatment, —and evidence of persistent disease in approximately 75% of patients with orthogonal diagnostic tools (serum prostate-specific antigen [PSA], magnetic resonance imaging [MRI]) suggested to us that the effect may not necessarily be due to (or foreshadow) tumor ablation. To this end, we proposed to more systematically study the pharmacologic effects of cabozantinib on the accumulation of bone-seeking radionuclides in tumor-naïve animals actively undergoing bone remodeling.

Methods

General Details

Cabozantinib was purchased from Selleck Chemicals (Houston, TX) and used without further purification. Axitinib and crizotinib were graciously provided by Pfizer, Inc. (New York, NY). Intact male CB17 SCID mice were acquired from Taconic Farms (Hudson, NY) at 3 to 6 weeks of age. ^{18}F–sodium fluoride (^{18}F-NaF) was purchased from the radiopharmacy at Memorial Sloan-Kettering Cancer Center (MSKCC). Radioactivity was measured for dose preparation using a Capintec CRC-15R Dose Calibrator (Capintec, Ramsey, NJ).

Induction of the Bone Fracture in Mice

All animal procedures were performed in compliance with Institutional Animal Care and Use Committee guidelines at MSKCC. Prior to surgery, intact male SCID mice were anesthetized with ketamine, and an incision was made in one hindlimb (in all cases, the contralateral limb was unmolested). The tibia was punctured using a handheld scalpel, whereupon the incision was sutured, and the animals received palliative doses of caprofen (5 mg/kg) once daily for 3 days postsurgery.

Serial Imaging with ¹⁸F-NaF Positron Emission Tomography during Therapy

Four to 7 days after the induction of the fracture, animals received 250 to 500 μCi of ¹⁸F administered intravenously via tail vein injection. One hour after the injection, mice were anesthetized by inhalation of a 1 to 2% isoflurane (Baxter Healthcare, Deerfield, IL)/oxygen gas mixture and placed on the scanner bed, and a 5- to 15-minute positron emission tomographic (PET) acquisition was performed to collect 20 million coincident events. PET imaging experiments were conducted on a microPET Focus 120 scanner (Concorde Microsystems, Knoxville, TN). Approximately 24 hours after the initial PET image, animals received an oral gavage of cabozantinib (30 mg/kg), axitinib (30 mg/kg), crizotinib (60 mg/kg), both axitinib and crizotinib, or vehicle. Cabozantinib was formulated in 1-methyl-2-pyrrolidone/PEG300 (1:10), axitinib was formulated in 0.5% w/v carboxylmethylcellulose (aq.), and crizotinib was formulated in water. Therapies were administered once daily for 7 days, except for axitinib, which was administered twice daily. Approximately 4 to 6 hours after the final gavage, the second ¹⁸F-NaF PET scan was conducted, and the animals were humanely euthanized.

Analysis of PET Imaging Data

List-mode data were acquired for between 10 and 30 minutes using a gamma-ray energy window of 350 to 750 keV and a coincidence timing window of 6 ns. Data were sorted into two-dimensional histograms by Fourier rebinning, and transverse images were reconstructed by filtered back-projection into a $128 \times 128 \times 63$ ($0.72 \times 0.72 \times 1.3$ mm) matrix. The image data were normalized to correct for nonuniformity of response of the PET, dead-time count losses, positron branching ratio, and physical decay to the time of injection, but no attenuation, scatter, or partial-volume averaging correction was applied. An empirically determined system calibration factor (in units of [mCi/mL]/[cps/voxel]) for mice was used to convert voxel count rates to activity concentrations. The resulting image data were then normalized to the administered activity to parameterize images in terms of %ID/g. Manually drawn two-dimensional regions of interest (ROI) were used to determine the maximum and mean %ID/g (decay corrected to the time of injection) in various tissues. Images were analyzed by using *ASIPro VM* software (Concorde Microsystems).

Serial Imaging with ⁹⁹ᵐTc-MDP during Therapy

A cohort of mice bearing tibial fractures was injected with ≈ 500 μCi of ⁹⁹ᵐTc-MDP. One hour after injection, the mice were anesthetized using 2 to 2.5% isofluorane with oxygen and placed on a NanoSPECT/CT scanner (Bioscan, Poway, CA). The gantry was equipped for constant flow of isofluorane/oxygen, and the bed was heated to 37°C. A computed tomographic (CT) topogram was acquired followed by a complete 360° microSPECT scan. Seven days after the initiation of therapy, a second scan was conducted following the same protocol. Bioscan *HiSPECT* software was used to reconstruct the imaging data and fuse the CT and SPECT images. The SPECT images were converted to raw data files and analyzed with ROI analysis using *ASIPro* software.

Results

To isolate the impact of cabozantinib on bone turnover in host tissues, we induced a fracture surgically in the tibiae of tumor-naïve intact male mice. The fracture was deliberately spaced away from knee and ankle joints to clearly resolve the wound site on the PET image. A pilot study was conducted to determine the onset of detectable bone remodeling by imaging a single cohort of injured animals at several time points postinjury. Although it was found that ^{18}F-NaF uptake could be detected 1 day after injury, we chose to image at 4 to 7 days postinjury, to allow the animals to acclimate to their wound (data not shown).

To determine the effects of cabozantinib on ^{18}F-NaF accumulation, a cohort of injured mice received a daily oral gavage of vehicle or a 30 mg/kg dose of cabozantinib for 7 days (30 mg/kg is a known bioactive dose in mice[10]). ROI analysis of the pre- and posttreatment PET scans showed a durable signal at the site of injury in animals treated with vehicle and a striking downregulation of radionuclide accumulation at the wound in animals treated with cabozantinib (Figure 1, A and B). No other obvious changes in the radionuclide accumulation could be detected by visually examining maximum-intensity projections. Moreover, no further suppression of radionuclide uptake was observed with a 80 mg/kg daily dosing regimen of cabozantinib (see Figure 1, A and B). A similar workflow was also applied to a separate cohort of animals assayed with ^{99m}Tc-MDP, and a marked decrease in radiotracer uptake was observed after cabozantinib therapy (Figure 1, C and D).

To attempt to define the RTKs responsible for this phenomenon, additional cohorts of animals bearing tibial fractures were treated with comparatively more selective RTK inhibitors. Because cabozantinib most potently inhibits vascular endothelial factor receptor (VEGFR) type 2 and MET, we chose to treat animals with crizotinib and axitinib, two highly promising inhibitors of the respective RTKs currently undergoing clinical evaluation.[11,12] We further chose to study the treatment effects with ^{18}F-NaF. The decision was motivated by the data showing clearer resolution of the site of bone remodeling with PET compared to SPECT with ^{99m}Tc-MDP, and because both radionuclides integrate within the hydroxyapatite lattice of bone via analogous diffusion-limited chemical mechanisms (^{99m}Tc-MDP integrates into the growing hydroxyapatite lattice via chemisorption, and fluoride-18 anion exchanges with exposed free hydroxyl groups).[13]

Interestingly, neither therapy impacted radionuclide accumulation compared to vehicle control as single agents, although doses known to be bioactive in preclinical tumor models were administered (Figure 2). These data raised the possibility that suppressing radionuclide accumulation may require simultaneous inhibition of several RTKs, a theory entirely plausible based on the fairly nonselective pharmacology of cabozantinib. Nevertheless, no bone scan resolution was observed in animals treated with both crizotinib and axitinib.

Discussion

In this study, we report the first evidence that bone scan resolution by systemic cabozantinib treatment can be a tumor-independent effect. Despite the challenges in reproducibly generating bone injuries of equal extent manually in small animals, cabozantinib treatment

suppressed ^{18}F-NaF or ^{99m}Tc-MDP uptake at the site of the fracture in all animal cohorts over the 2-year duration of this study. To deconvolute the biology of this phenomenon, two more selective VEGFR and MET inhibitors were studied in the same animal model, and no effect on ^{18}F-NaF was observed. Combination therapy also did not impact radionuclide accumulation, and to date, the molecular basis of bone scan resolution by cabozantinib in tumor-naïve mice remains elusive.

That neither VEGFR2 nor MET appears to be even partially implicated in this phenomenon is surprising for several reasons. Beyond being the "primary" targets of cabozantinib, there is evidence in the literature that leads one to reasonably hypothesize their role. For instance, the VEGF-VEGFR-hypoxia inducible factor signaling axis stimulates new vascularization into bone and neighboring cartilage, allowing the recruitment of osteoblast and osteoclast progenitors from the periosteum or bone marrow.[14] Perhaps consistent with this observation, partial to complete bone scan resolution was reported for a small percentage of CRPC patients treated with sunitinib, a therapy thought to exert its bioactivity primarily by inhibiting VEGFRs.[15, 16] Provocatively, bone scan resolution occurred independent of meaningful declines in serum PSA concentration or a response by Response Evaluation Criteria in Solid Tumors (RECIST), mirroring in part the clinical data reported for cabozantinib. Nevertheless (and much like cabozantinib), sunitinib potently inhibits multiple RTKs, and bone scan resolution by this drug cannot exclusively implicate the VEGFR family. The evidence involving MET is admittedly less direct; however, it is thought to contribute to prostate cancer metastasis to bone through stromal interactions, and elevated levels of MET expression have been reported in patient-derived tissue from bony mets.[17–19] Another consideration is that there is now compelling evidence in preclinical models that cabozantinib has direct antitumor effects, which reintroduces the possibility that some portion of the bone scan resolution is attributable to prostate cancer ablation.[5,10]

Collectively, the data reported in this study argue for a broader survey of single agents and drug combinations for other confirmed targets of cabozantinib to define the molecular basis of bone scan resolution, and we are currently working to this end. Understanding this mechanism could have immediate implications for the management of pain associated with bony metastases as a more selective drug (or combinations) could recapitulate the virtues of cabozantinib without its poor side effects.[20]

Acknowledgments

References

1. Yakes FM, Chen J, Tan J, et al. Cabozantinib (XL184), a novel MET and VEGFR2 inhibitor, simultaneously suppresses metastasis, angiogenesis, and tumor growth. Mol Cancer Ther. 2011; 10:2298–308.10.1158/1535-7163.MCT-11-0264 [PubMed: 21926191]

2. Bowles DW, Kessler ER, Jimeno A. Multi-targeted tyrosine kinase inhibitors in clinical development: focus on XL-184 (cabozantinib). Drugs Today. 2011; 47:857–68. [PubMed: 22146228]

3. Kurzrock R, Sherman SI, Ball DW, et al. Activity of XL184 (cabozantinib), an oral tyrosine kinase inhibitor, in patients with medullary thyroid cancer. J Clin Oncol. 2011; 29:2660–6.10.1200/JCO. 2010.32.4145 [PubMed: 21606412]

4. Sherman SI. Lessons learned and questions unanswered from use of multitargeted kinase inhibitors in medullary thyroid cancer. Oral Oncol. 2013; 49:707–10.10.1016/j.oraloncology.2013.03.442 [PubMed: 23582411]

5. Dai J, Zhang H, Karatsinides A, et al. Cabozantinib inhibits prostate cancer growth and prevents tumor-induced bone lesions. Clin Cancer Res. 2014; 20:617–30.10.1158/1078-0432.CCR-13-0839 [PubMed: 24097861]

6. Lee RJ, Saylor PJ, Michaelson MD, et al. A dose-ranging study of cabozantinib in men with castration-resistant prostate cancer and bone metastases. Clin Cancer Res. 2013; 19:3088–94.10.1158/1078-0432.CCR-13-0319 [PubMed: 23553848]

7. Smith DC, Smith MR, Sweeney C, et al. Cabozantinib in patients with advanced prostate cancer: results of a phase II randomized discontinuation trial. J Clin Oncol. 2013; 31:412–9.10.1200/JCO. 2012.45.0494 [PubMed: 23169517]

8. Dayyani F, Gallick GE, Logothetis CJ, Corn PG. Novel therapies for metastatic castrate-resistant prostate cancer. J Natl Cancer Inst. 2011; 103:1665–75.10.1093/jnci/djr362 [PubMed: 21917607]

9. Brown MS, Chu GH, Kim HJ, et al. Computer-aided quantitative bone scan assessment of prostate cancer treatment response. Nucl Med Commun. 2012; 33:384–94.10.1097/MNM. 0b013e3283503ebf [PubMed: 22367858]

10. Nguyen HM, Ruppender N, Zhang X, et al. Cabozantinib inhibits growth of androgen-sensitive and castration-resistant prostate cancer and affects bone remodeling. PloS One. 2013; 8:e78881.10.1371/journal.pone.0078881 [PubMed: 24205338]

11. Timofeevski SL, McTique MA, Ryan K, et al. Enzymatic characterization of c-Met receptor tyrosine kinase oncogenic mutants and kinetic studies with aminopyridine and triazolopyrazine inhibitors. Biochemistry. 2009; 48:5339–49.10.1021/bi900438w [PubMed: 19459657]

12. Liu G, Rugo HS, Wilding G, et al. Dynamic contrast-enhanced magnetic resonance imaging as a pharmacodynamic measure of response after acute dosing of AG-013736, an oral angiogenesis inhibitor, in patients with advanced solid tumors: results from a phase I study. J Clin Oncol. 2005; 23:5464–73.10.1200/JCO.2005.04.143 [PubMed: 16027440]

13. Wong KK, Piert M. Dynamic bone imaging with 99mTc-labeled diphosphonates and 18F-NaF: mechanisms and applications. J Nucl Med. 2013; 54:590–9.10.2967/jnumed.112.114298 [PubMed: 23482667]

14. Aleman J, Girotra M, Farooki A. Effects of tyrosine kinase inhibitors on bone metabolism. Endocr Relat Cancer. 201410.1530/ERC-12-0400

15. Saylor PJ, Mahmood U, Kunawudhi A, et al. Multitargeted tyrosine kinase inhibition produces discordant changes between 99mTc-MDP bone scans and other disease biomarkers: analysis of a phase II study of sunitinib for metastatic castration-resistant prostate cancer. J Nucl Med. 2012; 53:1670–5.10.2967/jnumed.112.105007 [PubMed: 22984218]

16. Dror Michaelson M, Regan MM, Oh WK, et al. Phase II study of sunitinib in men with advanced prostate cancer. Ann Oncol. 2009; 20:913–20.10.1093/annonc/mdp111 [PubMed: 19403935]

17. Knudsen BS, Gmyrek GA, Inra J, et al. High expression of the Met receptor in prostate cancer metastasis to bone. Urology. 2002; 60:1113–7.10.1016/S0090-4295(02)01954-4 [PubMed: 12475693]

18. Varkaris A, Corn PG, Gaur S, et al. The role of HGF/c-Met signaling in prostate cancer progression and c-Met inhibitors in clinical trials. Expert Opin Invest Drugs. 2011; 20:1677–84.10.1517/13543784.2011.631523

19. Pisters LL, Troncoso P, Zhau HE, et al. c-Met proto-oncogene expression in benign and malignant human prostate tissues. J Urol. 1995; 154:293–8.10.1016/S0022-5347(01)67297-5 [PubMed: 7539865]

20. Cho YT, Chan CC. Cabozantinib-induced hand-foot skin reaction with subungual splinter hemorrhages and hypertension: a possible association with inhibition of the vascular endothelial growth factor signaling pathway. Eur J Dermatol. 2013; 23:274–5. [PubMed: 23518371]
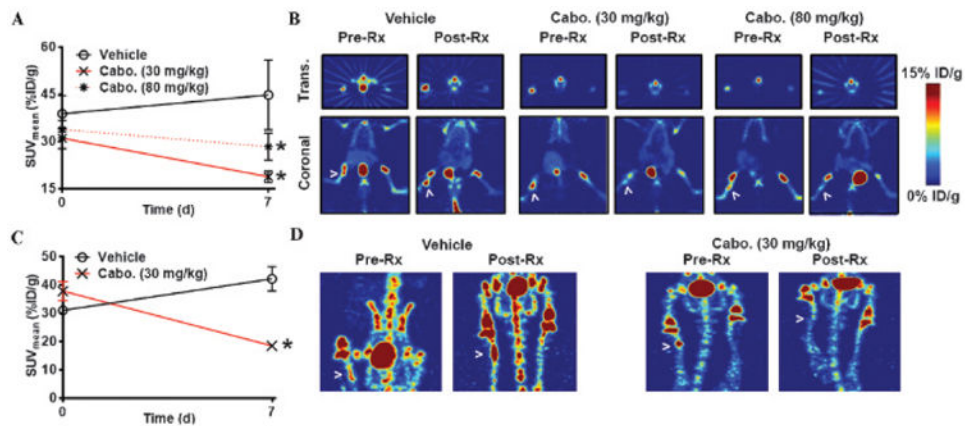
Figure 1.
A summary of the postcabozantinib (Cabo.) changes in bone-seeking radionuclide uptake at sites of remodeling bone. *A*, A line graph of the mean standardized uptake value (SUV_{mean}) for ^{18}F-NaF uptake at the site of the fracture in the tibia for three treatment arms shows the impact of cabozantinib therapy on radionuclide accumulation. Two doses, the lower of which was reported to be bioactive in tumor xenograft models, resulted in statistically significant declines in radionuclide uptake compared to vehicle control. No further decline in radionuclide accumulation was noted with the higher cabozantinib dose. *B*, Representative transverse (trans.) and coronal slices of mice incorporated in this study show visibly obvious changes in the intensity of the PET signal at the site of the fracture postcabozantinib therapy. The site of the fracture is indicated with a *white arrowhead*. *C*, A line graph of the SUV_{mean} for ^{99m}Tc-MDP uptake at the site of the fracture in the tibia shows the impact of cabozantinib therapy on radionuclide accumulation. Animals were treated once daily with cabozantinib at 30 mg/kg 1 day after the first SPECT scan. *D*, Representative maximum-intensity projection (MIP) images whose intensities were manually gated to provide a clear view of radionuclide uptake at the fracture site and the nearby anatomy. Quantification was not conducted using the MIP images; the MIP images are merely provided to show a global view of ^{99m}Tc-MDP distribution in the skeleton while underscoring the foci of high radionuclide uptake at the fracture. Unfortunately, centering the images on the slices with the fracture excluded the rest of the anatomy, resulting in images that are difficult to interpret visually. *$p < .01$. Rx = treatment.
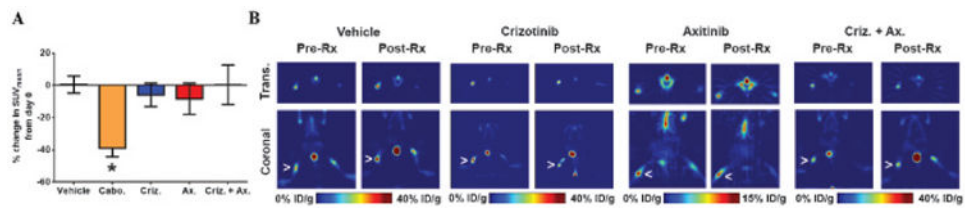
Figure 2.
A summary of the animal imaging data among all of the therapies used in this study. *A*, A bar graph shows the large reduction in radiotracer uptake at the site of the fracture after cabozantinib (Cabo.) therapy and no impact on radiotracer uptake among animals treated with crizotinib (Criz.), axitinib (Ax.), or the combination. The replicates per treatment are vehicle, $n = 30$; cabozantinib, $n = 20$; crizotinib, $n = 10$; axitinib, $n = 15$; crizotinib plus axitinib, $n = 15$. *B*, Representative transverse and coronal slices for each of the treatment arms, excluding cabozantinib, which was represented in Figure 1B. The position of the fracture is represented with an *arrowhead*. Note that the slices for one treatment arm (axitinib) are represented on a different intensity scale. All imaging data are available on request. *$p < .01$. Rx = treatment; SUVmean = mean standardized uptake value.